Hypersonic Rarefied Flow About Plates at Incidence

Virendra K. Dogra*
Vigyan Research Associates, Inc., Hampton, Virginia 23666
and
James N. Moss†
NASA Langley Research Center, Hampton, Virginia 23665

Results of a numerical study using the direct simulation Monte Carlo (DSMC) method are presented for the transitional flow about two plate configurations at incidence. Both plates are 12 m in length. One has zero thickness, and the other has a thickness of 0.5 m with a nose radius of 0.5 m. The flow conditions simulated are those experienced by the Space Shuttle Orbiter during re-entry at 7.5 km/s. The altitude range considered is that from 200 to 100 km, which encompasses most of the transitional flow regime for the Space Shuttle Orbiter. The DSMC simulations show that transitional effects are evident when compared with free-molecular results for all cases considered. These results demonstrate clearly that the transitional effects are significant even at those altitudes where the flow about a typical space vehicle has often been considered as free molecular. Therefore, it becomes very important to identify these transitional flow effects when making aerodynamic flight measurements of space vehicles as are currently being made with the Space Shuttle Orbiter vehicles. In the absence of calculations, previous flight data analyses have relied exclusively on the adjustments in the gas-surface interaction models without accounting for the transitional effects, which can be comparable in magnitude.

Nomenclature

C_d = drag coefficient, $2D/\rho_\infty V_\infty^2 \ell$
C_f = skin-friction coefficient, $2\tau/\rho_\infty V_\infty^2$
C_H = heat-transfer coefficient, $2q/\rho_\infty V_\infty^3$
C_l = lift coefficient, $2L/\rho_\infty V_\infty^2 \ell$
C_p = pressure coefficient, $2p/\rho_\infty V_\infty^2$
D = drag force
Kn_∞ = freestream Knudsen number, λ_∞/ℓ
L = lift force
ℓ = length of the flat plate
M = molecular weight of air
p = pressure
q = heat flux
R = universal gas constant, $R = 8.3143$ J/mol-K
R_N = nose radius
S_∞ = freestream speed ratio, $V_\infty \sqrt{M/2RT_\infty}$
T = thermodynamic temperature
T_∞ = freestream temperature
T_w = surface temperature
u = velocity component tangent to the plate surface
V_∞ = freestream velocity
v = velocity component normal to the plate surface
x_i = mole fraction of species i
x = coordinate measured along the plate
y = coordinate measured normal to the plate
α = angle of incidence
ε = fraction of specular reflection
η = exponent in inverse power law model
λ_∞ = freestream mean free path
ρ = density
σ = collision cross section
τ = skin friction
ω = viscosity-temperature exponent

Subscripts
i = ith species
ref = standard conditions at 160-km altitude
w = surface values
∞ = freestream values

Abbreviations
DSMC = direct simulation Monte Carlo
FM = free molecular
VSH = variable hard sphere

Presented as Paper 89-1712 at the AIAA 24th Thermophysics Conference, Buffalo, New York, June 12–14, 1989; received June 29, 1989; revision received Jan. 14, 1991; accepted for publication Feb. 27, 1991.

*Research Engineer. Member AIAA.
†Research Engineer. Fellow AIAA.

Introduction

ACCURATE predictions of aerothermal loads during re-entry can be very important for the design and development of hypersonic space vehicles. A portion of the re-entry for these vehicles takes place in the transitional flow regime where various nonequilibrium effects become important in establishing the thermal and aerodynamic response of these vehicles. In order to simplify the computational requirements, the aerothermal loads for vehicles such as the Space Shuttle Orbiter are often approximated[1,2] with a flat plate at incidence for the free-molecular flow regime. For the transitional flow regime, empirical approximations are normally used to calculate these loads.[1-3] It has been observed from the Space Shuttle's flight experiments that measurd values of lift/drag ratio are considerably higher than the free-molecular flow calculations at altitudes of 160 km and above where the flow regime was believed to be free molecular. This discrepancy is thought to be due to specular reflection of some fraction of the molecules at the surface. As early as 1985, it was recognized[4] that transitional effects rather than specular gas–surface interaction might be influencing the interpretation of the flight measurements; however, no calculations were available to establish this hypothesis.

Recent direct simulation Monte Carlo (DSMC) calculations[5] of the rarefied flow past a flat plate at incidence were the first to show that the transitional effects persist for the Space Shuttle Orbiter even at altitudes (160 km and above) where the flow had previously been considered as free molecular. In these calculations, a 1-m flat plate of zero thickness and 40 deg incidence was used to simulate the freestream Knudsen

number of the Space Shuttle Orbiter during re-entry. For example, this study showed that the transitional effects at a freestream Knudsen number of 8.4 would increase the Space Shuttle Orbiter lift/drag ratio by 90% over the free-molecular value. Thus, the interpretation of aerodynamic flight data for space vehicles at high altitudes must be done in concert with calculations that describe the transitional effects. Failure to account for this effect could significanty distort the interpretation of the gas–surface interactions under highly rarefied conditions.

Numerical studies on basic configurations such as a plate at incidence can provide useful information and physical insight concerning the nature of transitional flows. Therefore, the flat plate as a basic aerodynamic surface has remained the focus of the rarefied flow research by several authors.[6–10] But most of these investigations are for zero incidence and do not cover the range of flow parameters of interest. There are very few experimental and theoretical investigations[11–13] for the flat plate at incidence. Even these do not cover the large incidence and high-speed ratio characteristics of hypersonic flight.

To obtain further insight into the transitional flow effects on the aerothermal loads of space vehicles during re-entry, DSMC simulations of the rarefied flow about two plate configurations were made in the present study. One plate had zero thickness, whereas the second had a thickness of 0.5 m and a blunted leading edge (nose radius = 0.5 m). Both plates were 12 m in length, which corresponds to the mean aerodynamic cord of the Shuttle Orbiter's wings. DSMC calculations were made for an altitude range of 200 to 100 km at 7.5 km/s using a five-species reacting air model. Angles of incidence considered were 20–80 deg, where the primary focus was 40 deg, which corresponds to the nominal incidence of the Shuttle Orbiter during the transitional flow portion of its re- entry.

Computational Approach

The DSMC method[14–15] models the real gas by some thousands of simulated molecules in a computer. The position coordinates, velocity components, and internal state of each molecule are stored in the computer and are modified with time as the molecules are concurrently followed through representative collisions and boundary interactions in simulated physical space. The time parameter in the simulation may be identified with physical time in the real flow, and all calculations are unsteady. When the boundary conditions are such that the flow is steady, then the solution is the asymptotic limit of unsteady flow. The computation is always started from an initial state that permits an exact specification such as a vacuum or uniform equilibrium flow. Consequently, the method does not require an initial approximation to the flowfield and does not involve any iterative procedures. A computational cell network is required in physical space only, and then only to facilitate the choice of potential collision pairs and the sampling of the macroscopic flow properties. Furthermore, advantage may be taken of flow symmetries to reduce the dimensions of the cell network and the number of position coordinates that need to be stored for each molecule, but the collisions are always treated as three-dimensional phenomena. The boundary conditions are specified in terms of the behavior of the individual molecules rather than the distribution functions. All procedures may be specified in such a manner that the computational time is directly proportional to the number of simulated molecules.

Conditions for Calculations

The freestream conditions considered in the present study are those experienced by the Space Shuttle Orbiter during re-entry from 200- to 100-km altitude range. Two plate configurations are used for the flow simulation: 1) a flat plate with zero thickness and 2) a blunt plate with a nose radius of 0.5 m and a thickness of 0.5 m. The length of both plates is equal to the mean aerodynamic chord (12 m) of the Space Shuttle Orbiter wings. These configurations are shown in Fig. 1. The freestream conditions and parameters along with selected results are summarized in Tables 1 and 2. The atmospheric conditions are those given by Jacchia[16] for an exospheric temperature of 1200 K.

The surface temperature is assumed to be constant along the surface and equal to the wall radiative equilibrium value on the windward side (evaluated with free-molecular heating and a surface emittance of 0.9). Also, the wall is assumed to be diffuse with full thermal accommodation and to promote recombination of the oxygen and nitrogen atoms. The oxygen and nitrogen recombination probabilities are assumed to be 0.0049 and 0.0077, respectively.

The chemical kinetics model for the calculations is the same as that used in Refs. 17 and 18 (the species O_2, N_2, O, N, and NO with 34 chemical reactions). Since the computational requirements increase significantly with increasing freestream density, the computations are not performed below 100-km altitude.

Results and Discussion

Attention is focused on the flow structure, surface quantities, and aerodynamic characteristics resulting from hypersonic low-density flow past two plate configurations at incidence. A previous study[1] has shown that a flat plate at 40-deg incidence provides a good approximation to the free-molecular lift-to-drag (L/D) ratio of the Shuttle Orbiter. Simulation of the flow about a plate configuration reduces the computational task compared to that of the three-dimensional flow about the orbiter and still provides important information concerning the transitional flow effects at high altitudes for the Shuttle Orbiter. Furthermore, the plate is a basic configuration often used for experimental and numerical simulations to study the physics of rarefied flows.

Flowfield Structure

The flowfield environment is of prime interest for understanding the flow phenomena that contribute to the surface quantities. Furthermore, when comparing the results of different numerical methods, the flowfield structure becomes invaluable. Therefore, the present section emphasizes the flowfield structure as calculated with the DSMC method.

Figure 2 presents the calculated flowfield quantities on the compression side (lower surface) of the flat plate for the 100-km altitude case. Results at three different locations along the surface are presented. Near the surface, a large increase in density occurs (Fig. 2a) which is characteristic of high-speed flows about a cold wall. This increase in density near the wall for a given freestream condition and wall temperature gradually increases with incidence angle and becomes maximum for the surface perpendicular to the flow. Figure 2c clearly demonstrates that there is not a distinct shock wave for the 100-km altitude case (kn_∞ = 0.01), only the situation where the shock wave merges with the shock layer. The thickness of the flowfield disturbance gradually increases with distance

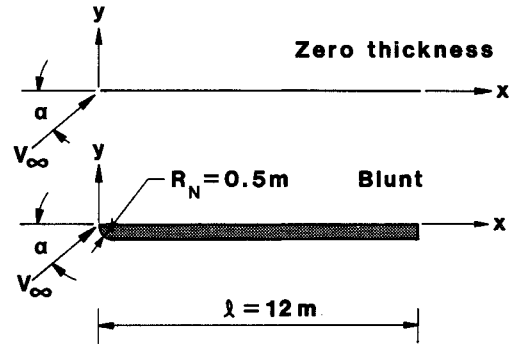

Fig. 1 Plate configurations.

Table 1 Freestream conditions

Altitude, km	ρ_∞, kg/m^3	V_∞, km/s	T_∞, K	Mole fraction X_{O_2}	Mole fraction X_{N_2}	Mole fraction X_O	$\overline{M}$, g/mol	λ_∞, m
200	3.29×10^{-10}	7.5	1025.8	0.031	0.455	0.514	21.97	190.510
180	6.13×10^{-10}	7.5	946.8	0.039	0.516	0.444	22.83	101.670
160	1.320×10^{-9}	7.5	821.5	0.049	0.581	0.370	23.76	49.149
140	3.860×10^{-9}	7.5	625.2	0.062	0.652	0.286	24.82	17.555
120	2.270×10^{-8}	7.5	367.8	0.084	0.733	0.183	26.16	3.146
100	5.641×10^{-7}	7.5	194.3	0.177	0.784	0.039	28.26	0.137

Table 2 Various parameters and results

Altitude, km	Kn_∞	S_∞	T_w, K	Aerodynamic coefficient C_L	Aerodynamic coefficient C_D	Aerodynamic coefficient L/D	q,[a] kW/m^2
(a) *Flat plate at 40-deg incidence*							
200	15.876	8.7	175	0.13	1.30	0.10	0.044
180	8.472	9.0	202	0.17	1.29	0.13	0.088
160	4.096	9.9	245	0.23	1.26	0.18	0.163
140	1.462	11.6	319	0.31	1.15	0.27	0.434
120	0.262	15.5	495	0.46	1.05	0.44	1.870
100	0.011	22.2	1100	0.64	0.77	0.83	13.300
(b) *Blunt plate at 40-deg incidence*							
160	4.096	9.9	245	0.22	1.33	0.16	0.170
140	1.462	11.6	319	0.32	1.28	0.25	0.442
120	0.262	15.5	495	0.45	1.1	0.41	1.86
100	0.011	22.2	1100	0.62	0.80	0.77	11.6

[a]Approximately at the center of the lower surface.

along the surface. For the higher altitude cases, the extent of the flowfield disturbances is much larger because of the higher degree of rarefaction.

The overall nondimensional kinetic temperature T/T_∞ (Fig. 2c) is defined for a nonequilibrium gas as the weighted mean of the translational and internal temperatures. Figure 2c shows that the overall kinetic temperature rise in the shock wave precedes the density rise. The initial rise in temperature is due to the bimodal velocity distribution where the molecular samples consist of mostly undisturbed freestream molecules with just a few molecules that have been affected by the shock. The large velocity separation between these two classes of molecules results in the early temperature increase.

The temperature rise in the shock wave is comparatively large near the leading edge and then gradually decreases toward the trailing edge (Fig. 2c). The temperature and velocity profiles also show the extent of the temperature jump and the velocity slip at 100-km altitude (Figs. 2c and 2b).

Surface Quantities

The effect of including plate thickness on the surface quantities is considered first for the two plate geometries at 40-deg incidence. Comparisons of surface quantities along the lower surface are presented in Figs. 3 and 4 for the 100- and 160-km cases, respectively. The pressure and heat-transfer coefficients have their maximum value at the stagnation point for the blunted leading edge plate, whereas the skin friction is zero. For the 100-km case, the nose significantly affects the surface quantities downstream of the tangency point (Fig. 3). Yet, at 160 km, the flow is sufficiently rarefied such that the blunt nose has no effect on the surface quantities downstream of the tangency point (Fig. 4). Therefore, the influence of a leading edge on an afterbody surface would be confined to the leading edge.

The effects of rarefaction can be seen by comparing the results for the flat plate for two altitudes (100 and 160 km) from Figs. 3 and 4. The variation of the pressure coefficient with rarefaction is moderate provided the gas–surface interaction is diffuse, as assumed in the present calculations. In contrast, the skin-friction and heat-transfer coefficients are very sensitive to rarefaction effects and approach the free-molecular value with increasing altitude.

The effect of wall temperature on the surface quantities of a flat plate at 160-km altitude is shown in Fig. 5. Figures 5a and 5b show that the pressure and skin-friction coefficients increase moderately with increasing wall temperature. The increase in pressure is primarily due to the increase in normal momentum of the reflected molecules with increasing wall temperature. The skin friction only depends on the tangential momentum of the incident flux for diffused reflection. With increasing surface temperature, the reflected molecules attain more energy, and their collisions with other molecules increase the incidence flux as well as the tangential momentum, which results in a moderate increase of skin friction. In contrast, the heat-transfer coefficient (Fig. 5c) decreases with increasing surface temperature because more energy is carried away by the reflected molecule flux as the surface temperature increases.

Figures 6a to 6c show the effect of gas–surface interaction on the surface quantities. Three combinations of specular and diffuse surface reflection are considered, ranging from fully diffuse to 25% specular. It can be seen from Fig. 6a that the pressure coefficient increases significantly with increasing specular reflection. This increase in the pressure is due to the increase in the normal momentum of the reflected molecules as the percentage of specular reflection goes up. Figures 6b and 6c show the extent that the skin-friction and heat-transfer coefficients decrease as the percentage of specular reflection increases.

The effect of the molecular gas model on surface quantities is presented in Fig. 7 where the variable hard sphere (VSH) model is used with three different viscosity-temperature relations ω. In the current implementation of the VHS model, a single value of ω is used regardless of the number of chemical species considered in the simulation. The value of ω used in the present study ($\omega = 0.73$) provides excellent agreement with the viscosity data suggested by Biolsi[19] for diatomic nitrogen. For the other four species considered in the gas model, the agreement with the viscosity data of Biolsi is good with

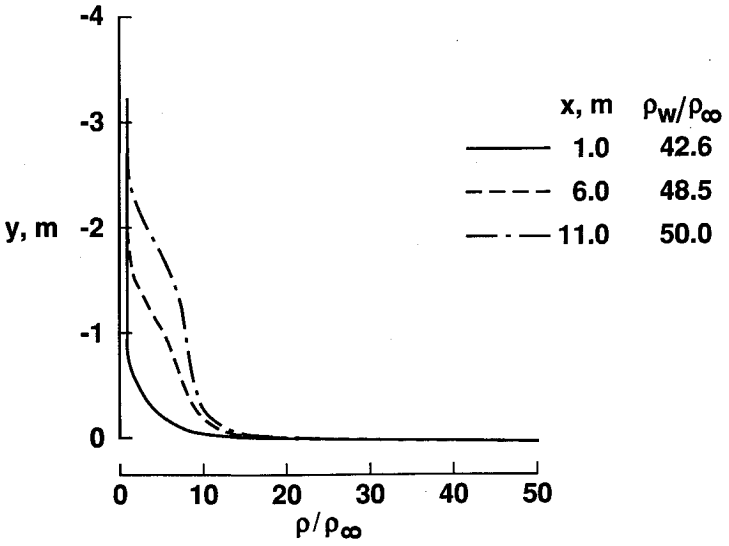

a) Density profiles

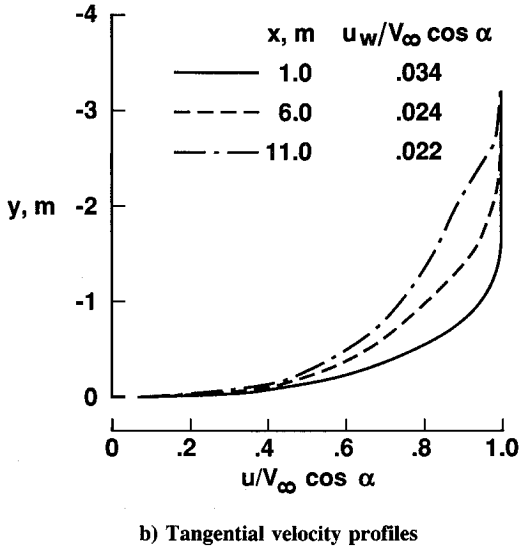

b) Tangential velocity profiles

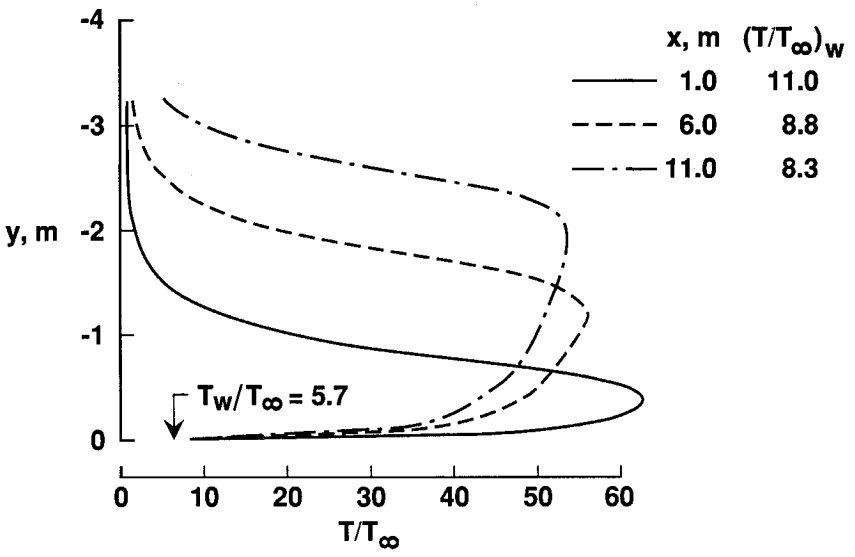

c) Overall kinetic temperature profiles

Fig. 2 Flowfield structure along the lower surface of the flat plate (Alt = 100 km, V_∞ = 7.5 km/s, Kn_∞ = 0.01, T_w = 1100 K, α = 40 deg).

the exception of atomic nitrogen whose concentration is insignificant in the present application.

Three quantities describe the VHS model for each chemical species: a reference diameter or cross section, a reference temperature, and the viscosity-temperature exponent. The reference temperature used in the present calculations was 2880 K, and the reference diameters at the reference temperature are listed in Table 3 for each of the five species considered. The elastic cross section for a nonequilibrium gas is given by

$$\sigma = \sigma_{ref}[C_r^2/[C_r^2]_{ref}]^{-(\omega-0.5)}$$
$$= \sigma_{ref}[C_r^2/[C_r^2]_{ref}]^{-2/(\eta-1)}$$

where C_r is the relative velocity of the colliding particles and "ref" designates a reference state. The relation between ω and the exponent of the inverse power law molecular force η, is given by

$$\omega = \frac{\eta + 3}{2(\eta - 1)}$$

where the force is inversely proportional to the molecular separation distance raised to the power of η.

In considering the effect of the molecular model, two additional values of ω were used: 0.5 and 1.0. These are two fictitious models that have different temperature-viscosity relations (consequently, different cross sections and collision frequencies) than the more realistic model with ω = 0.73. For ω = 0.5, we have a model where each chemical species has a constant elastic cross section equal to its reference value. If the gas consisted of only monatomic species, the ω = 0.5 model would be a hard sphere model that could be regarded as the special limiting case of the inverse power law model with $\eta = \infty$. If we were considering a single species monatomic gas, then the model for ω = 1.0 would correspond to a Maxwell model, which is a special case of the inverse power law model with η = 5. The collision probability of a molecule in a Maxwellian gas is independent of its velocity, which is the major analytical advantage of the Maxwell molecule.

To the extent that a real monatomic molecule is properly represented by the inverse power law model, the effective value of η is generally around 10. The special cases of hard-sphere and Maxwell molecules provide useful limiting cases

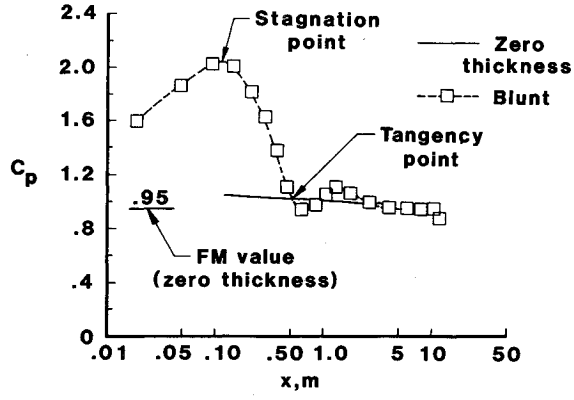

a) Pressure coefficient

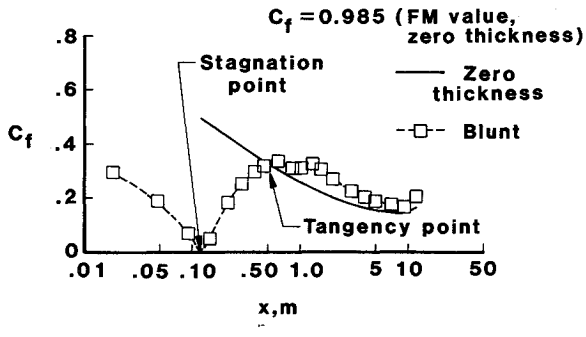

b) Skin-friction coefficient

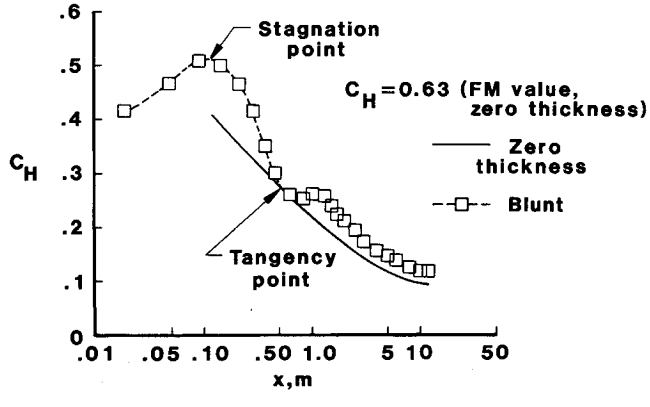

c) Heat-transfer coefficient

Fig. 3 Comparison of surface quantities (Alt = 100 km, V_∞ = 7.5 km/s, Kn_∞ = 0.01, T_w = 1100 K, α = 40 deg).

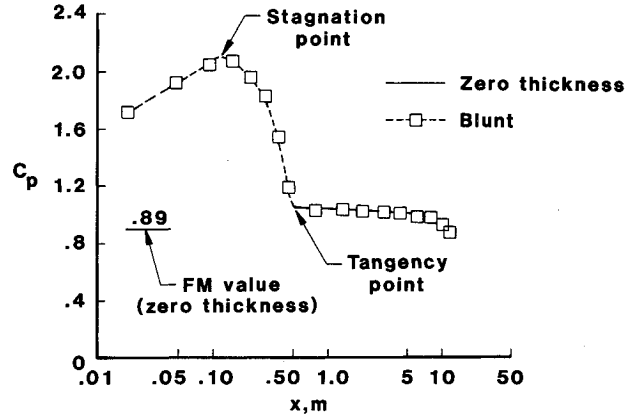

a) Pressure coefficient

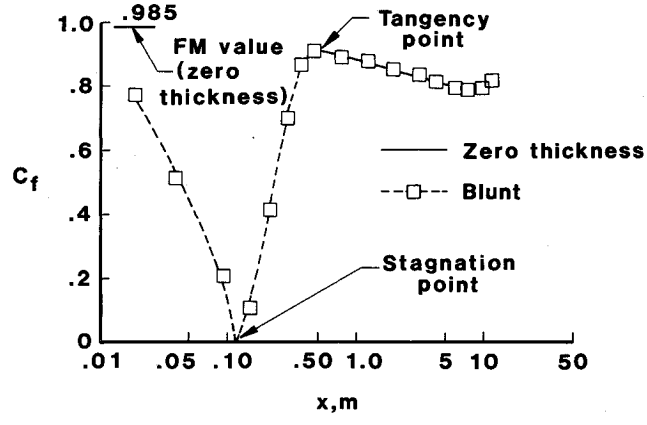

b) Skin-friction coefficient

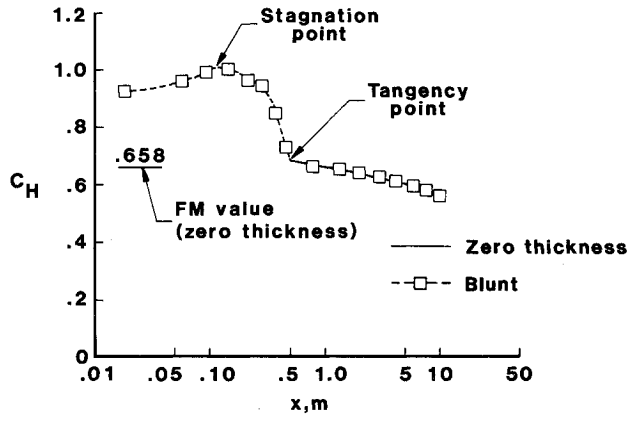

c) Heat-transfer coefficient

Fig. 4 Comparison of surface quantities (Alt = 160 km, V_∞ = 7.5 km/s, Kn_∞ = 4.0, T_w = 245 K, α = 40 deg).

Table 3 VHS molecular diameters at 2880 K

	ω		
	0.50	0.73[a]	1.0
Species	Diameter, m × 10^{10}		
O_2	2.86	3.06	3.44
N_2	2.88	3.08	3.46
O	2.14	2.30	2.58
N	2.24	2.40	2.70
NO	2.86	3.06	3.44

[a]The value of ω that provides the desired viscosity-temperature relation.

for "hard" and "soft" molecules, respectively. The effective value of η is generally established through the temperature dependence of the coefficient of viscosity.[15] Theory based on the power law model provides a temperature exponent that is a function of η only. In the present study with the VHS model, the temperature power used to model the viscosity dependence on temperature was 0.73, which corresponds to an η value of 9.7. (See Eq. 5 of Ref. 14.)

There is overwhelming evidence that the observable effects due to changes in molecular model are produced by the different variations with temperature (for an equilibrium gas or

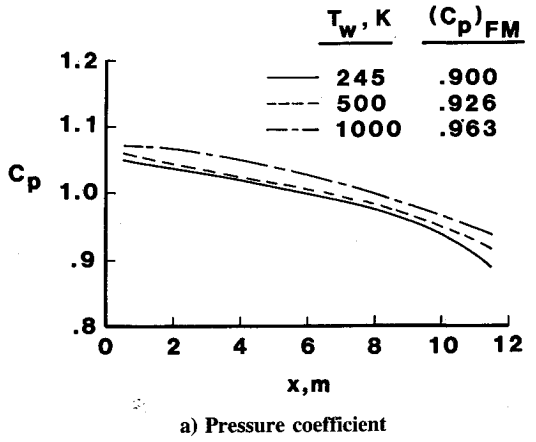

a) Pressure coefficient

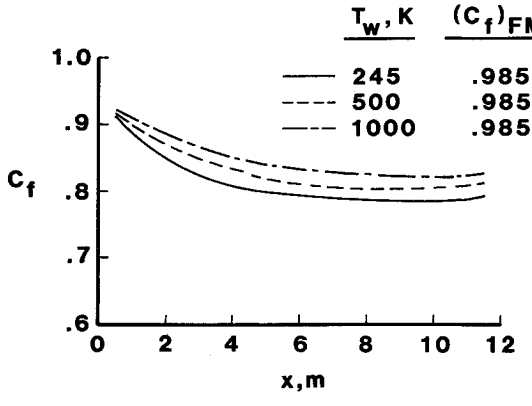

b) Skin-friction coefficient

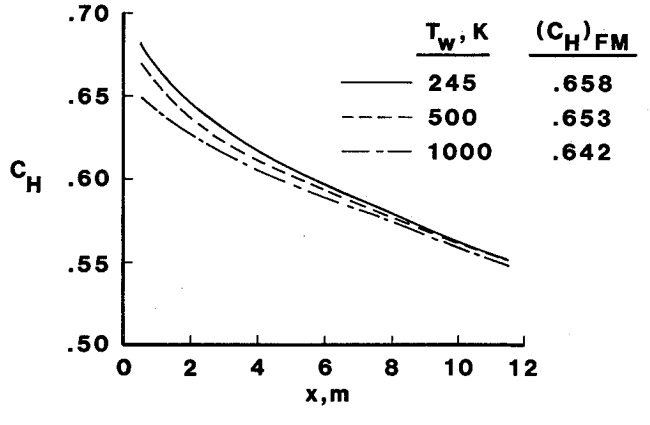

c) Heat-transfer coefficient

Fig. 5 Effect of wall temperature on surface quantities of the flat plate (Alt = 160 km, V_∞ = 7.5 km/s, Kn_∞ = 4.0, α = 40 deg).

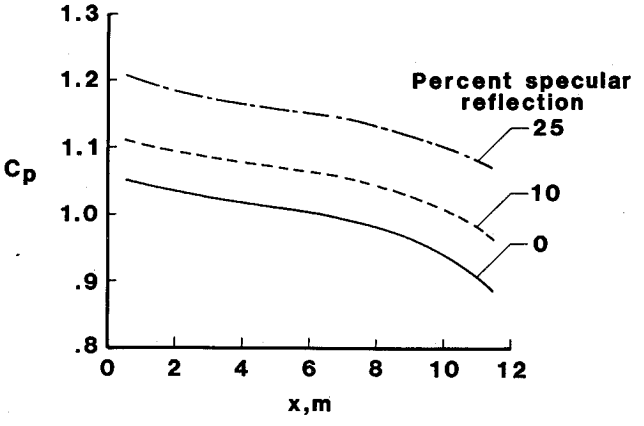

a) Pressure coefficient

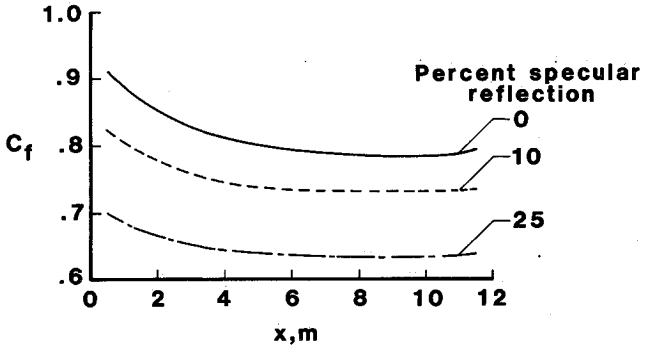

b) Skin-friction coefficient

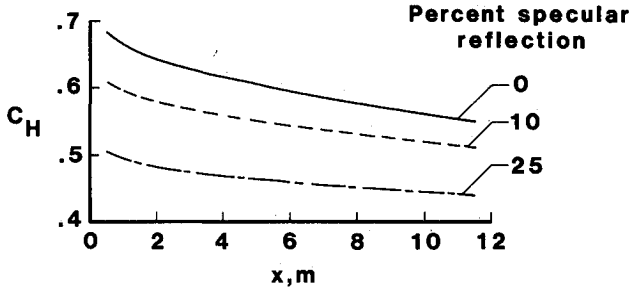

c) Heat-transfer coefficient

Fig. 6 Effect of gas surface interaction on the surface quantities of the flat plate (Alt = 160 km, V_∞ = 7.5 km/s, Kn_∞ = 4.0, α = 40 deg).

relative velocity for a nonequilibrium gas) of the collision cross section.[14] The VHS model is the recommended model[14] for simulating monatomic gases in an engineering context, since the VHS model combines the simplicity of the hard-sphere scattering law with a variable cross section.

The departure of the surface quantities from those obtained with the VHS model using a realistic value of ω can be seen in Fig. 7 for the two limiting cases of ω = 0.5 and ω = 1.0 models. Note that the common basis for these comparisons is that the viscosity at the reference temperature (2800 K) is the same. Consequently, the reference collision cross section is also different for each of the three gas models. (See Eq. 14 or Ref. 14.) In general, the VHS results with ω = 0.73 are bounded by the results obtained with ω = 0.5 and 1.0. The maximum differences with respect to the VHS model with ω = 0.73 are less than 6% for pressure, skin-friction, and heat-transfer coefficients.

Aerodynamic Characteristics

Figures 8 and 9 present the variation in aerodynamic characteristics as a function of freestream Knudsen number. Figure 8 presents a comparison of these values for the flat plate

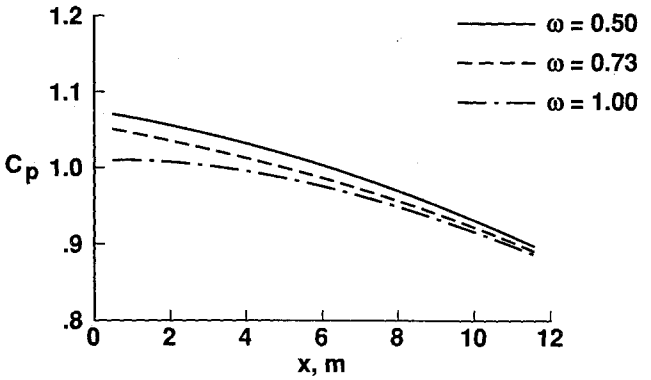

a) Pressure coefficient

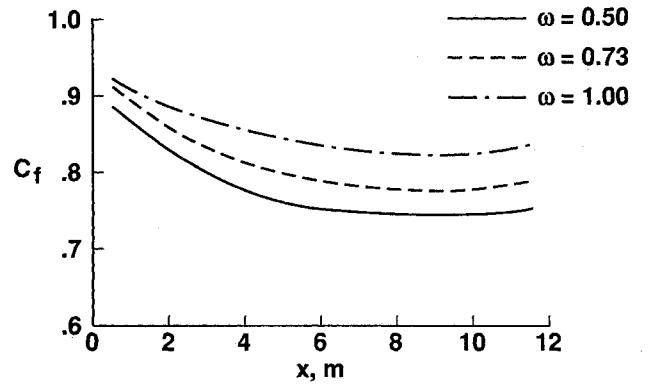

b) Skin-friction coefficient

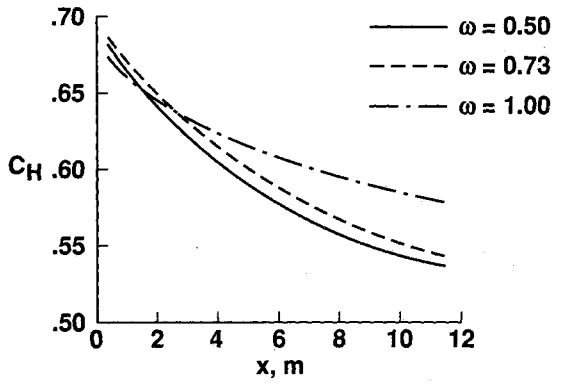

c) Heat-transfer coefficient

Fig. 7 Effect of molecular model on the surface quantities of the flat plate (Alt = 160 km, V_∞ = 7.5 km/s, Kn_∞ = 4.0, α = 40 deg).

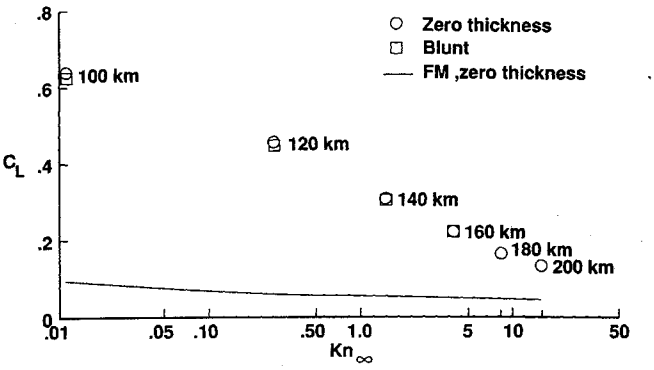

a) Lift coefficient

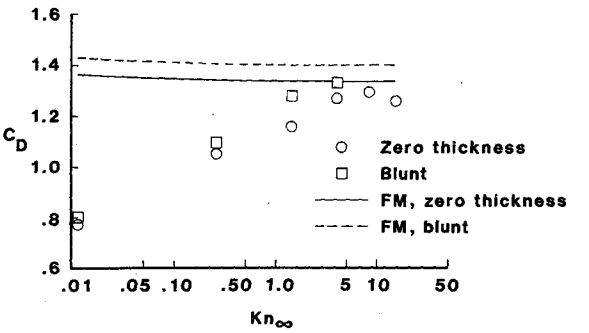

b) Drag coefficient

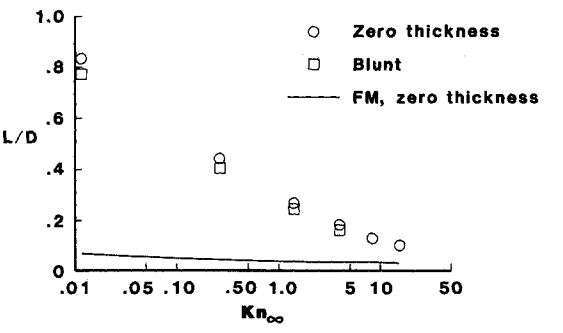

c) Lift/drag ratio

Fig. 8 Effect of rarefaction on aerodynamic characteristics (V_∞ = 7.5 km/s, α = 40 deg).

and the blunt plate at 40-deg incidence. These results show the expected variation in the transitional flow regime for both plates. The drag coefficient increases and the lift coefficient decreases substantially with increasing rarefaction; both approach the free-molecular limit. The lift coefficient (Fig. 8a) for both plates is practically the same; however, at the lower values of Knudsen number, the C_L values for the blunt plate are slightly lower than the flat plate values because of the nose thickness and the downstream influence of the blunt leading edge. As expected, the drag coefficient is slightly higher for the blunt plate as compared to the flat plate, and this is due to the plate thickness effect (Fig. 8b). Figure 8c presents the lift/drag ratio as a function of freestream Knudsen number for both plates. The lift/drag ratio behaves in the same way as the lift coefficient data, which experience significant decrease with increasing rarefaction.

Figure 9 presents the calculated lift and drag coefficients for the flat plate as a function of freestream Knudsen number along with the corresponding free-molecular results. For a freestream Knudsen number of 16, the lift and drag coefficients have not attained their free-molecular values.

The effect of angle of incidence variation of the aerodynamic coefficient is demonstrated in Fig. 10 for the flat plate at 160-km altitude. The DSMC results are compared with

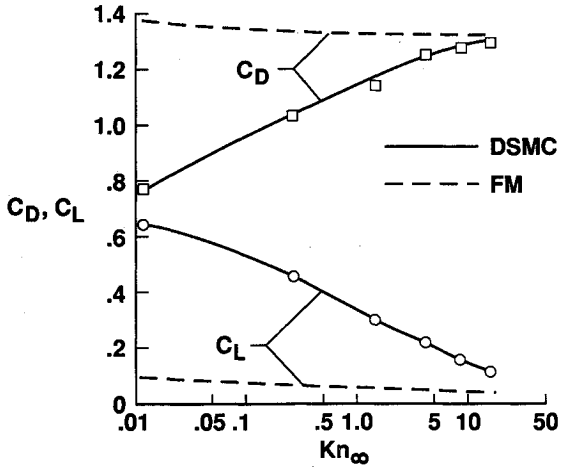

Fig. 9 Comparison of lift and drag coefficients for the flat plate (V_∞ = 7.5 km/s, α = 40 deg).

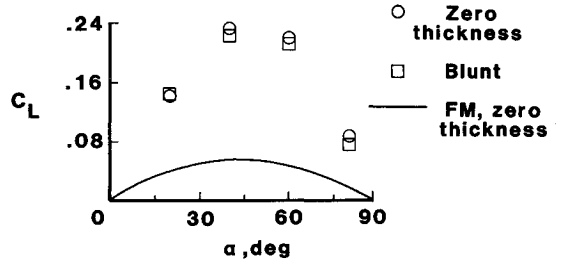

a) Lift coefficient

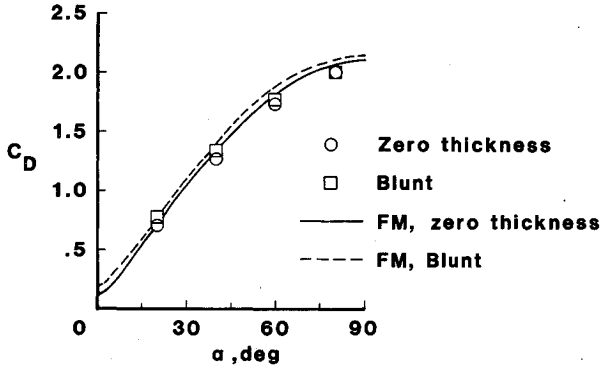

b) Drag coefficient

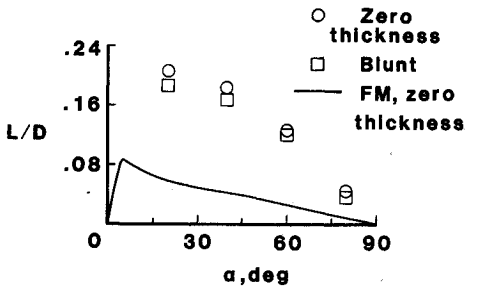

c) Lift/drag ratio

Fig. 10 Variation of aerodynamic characteristics with angle of incidence (Alt = 160 km, V_∞ = 7.5 km/s, Kn_∞ = 4.0, T_w = 245 K, α = 40 deg).

those obtained using free-molecular expressions for lift and drag coefficients and lift/drag ratio. Figure 10a shows that the lift coefficient for both plates increases with angle of attack, reaches a maximum value near 45 deg, then decreases with further increase in angle of attack. The DSMC values are considerably higher than the free-molecular values, indicating that transitional effects are evident even at this altitude where the freestream Knudsen number is 4. Figure 10b shows that the drag coefficient agrees well with the free-molecular calculations for small incidence. However, at higher incidence the DSMC values are slightly lower than the free-molecular values because of the overprediction of skin friction by the free-molecular method. Figure 10c presents the corresponding lift/drag ratio comparison for both plates and shows the same trend of the transitional effects as in the lift coefficient data.

These results have important implications for the interpretation of flight measurements used to deduce aerodynamic coefficients under rarefied conditions. It was recognized[4] that transitional effects rather than specular reflection might be influencing the interpretation of the flight measurements; however, no calculations were available to establish the fact. At altitudes of 160 km and above, the conventional procedure[1-3] has been to interpret the flight measurements using the free-molecular flow calculations. Such procedures are used to establish what fraction of the gas–surface interaction is specular. But it can be seen from the present calculations that the transitional effects persist even at very high altitudes (160 km and above). This is clearly demonstrated in Fig. 10c where the transitional effect increases the lift/drag ratio by 337% for a flat plate at 40-deg incidence. The freestream Knudsen number for this condition is 4.09, which corresponds to a Shuttle Orbiter re-entry condition at 160 km. This transitional effect is quite large and, if not properly interpreted, could be mistaken for a contribution due to specular reflection. As the fraction of specular reflection increases, the lift/drag ratio also increases for a given incidence angle. Since these two separate effects both produce increased lift/drag ratio, interpretation of flight measurements must account for the transitional effects.

Another important consideration in performing calculations of aerodynamic coefficients is the accuracy of the freestream density. It has been observed in the Space Shuttle flight experiments[20] that at higher altitudes (above 100 km), the fluctuations in the standard atmospheric density are of the order of ± 50%. (See Fig. 4 of Ref. 20.) The effect of a ± 50% variation in the freestream density will have a significant impact on the calculated aerodynamic coefficients. This is illustrated by the tabulated results in Table 4 where the lift, drag, and lift-to-drag ratio for specified fluctuations in freestream density are normalized by their respective standard values. These results are for 160-km altitude and a flat plate of 40-deg incidence. When the freestream density is 50% higher than the standard value, the lift force is 73% higher, the drag is 47% higher, and the L/D ratio is 17% higher. When the freestream density is 50% lower than the standard value, the lift force is 62% lower, the drag is 49% lower, and the L/D ratio is 25% lower. Consequently for meaningful comparisons to be made between flight experiments and calculations, it is imperative that the freestream density be defined with some precision. Although the L/D ratio can be obtained from the accelerometer measurements without

Table 4 Effect of freestream density variations on aerodynamic characteristics[a]

$\rho/(\rho)_{ref}$	$L/(L)_{ref}$	$D/(D)_{ref}$	$\frac{L/D}{(L/D)_{ref}}$
1.5	1.73	1.47	1.17
0.5	0.38	0.51	0.75

[a]Flat plate at 40-deg incidence and 160 km.

knowledge of the freestream density, the freestream density must be known accurately to do a meaningful calculation.

Recent development of the three-dimensional DSMC codes by Bird,[21] subsequent to the present study, has produced a set of codes which make it possible to compute the rarefied flow about complex three-dimensional shapes. Reference 21 presents results of simulations of the flow environment about the full Shuttle Orbiter for altitudes of 120 to 170 km. Comparison of the three-dimensional results with the flight measured L/D values confirm the present findings that the flight measurements are consistent with full diffuse reflection and that rarefaction effects persist to altitudes significantly greater than 200 km for vehicles as large as the Shuttle Orbiter.

Concluding Remarks

Results obtained with DSMC method for two plate configurations at incidence show that the flowfield is rarefied, and transitional effects persist for all the cases considered. At lower altitudes, the nose significantly affects the surface quantities downstream of the tangency point of the plate. As the rarefaction increases, the influence of the nose is confined more and more to the leading edge. The transitional effects on aerodynamic characteristics are significant even for large freestream Knudsen numbers. Thus, the interpretation of aerodynamic flight data for space vehicles must be done in concert with the calculations that describe the transitional effects. However, any comparison of the flight experimental data with the numerical calculations is only possible if the freestream conditions are accurately measured. Failure to obtain accurate freestream conditions would make comparisons of numerical results with flight measurements meaningless.

References

[1]Blanchard, R. C., "Rarefied Flow Lift-to-Drag Measurements of the Shuttle Orbiter," 15th Congress of International Council of Aeronautical Sciences, Paper ICAS-86-2.10.1, London, England, September 7–12, 1986.

[2]Blanchard, R. C., Hendrix, M. K., Fox, J. C., Thomas, D. J., and Nicholson, J. Y., "Orbital Acceleration Research Experiment," *Journal of Spacecraft and Rockets*, Vol. 24, No. 6, 1987.

[3]*Aerodynamic Design Data Book*, Vol. 1, Orbiter Vehicle 102, SD72-SH-0060, Vol. 1M, Space Division, Rockwell International, Nov. 1980.

[4]Blanchard, R. C., and Rutherford, J. F., "Shuttle Orbiter High Resolution Accelerometer Package Experiment: Preliminary Flight Results," *Journal of Spacecraft and Rockets*, Vol. 22, No. 4, 1985, pp. 474–480.

[5]Dogra, V. K., Moss, J. N., and Price, J. M., "Rarefied Flow Past a Flat Plate at Incidence," *Rarefied Gas Dynamics*, edited by E. P. Muntz, D. P. Weaver, and D. H. Campbell, Vol. 118, Progress in Astronautics and Aeronautics, AIAA,1988, pp. 567–581.

[6]Vogenitz, F. V., Broadwell, J. E., and Bird, G. A., "Leading Edge Flow by Monte Carlo Direct Simulation Technique," *AIAA Journal*, Vol. 8, No. 3, 1971, pp. 304–310.

[7]Vogenitz, F. V., and Takata, G. Y., "Rarefied Gas Flow About Cones and Flat Plates by Monte Carlo Simulation," *AIAA Journal*, Vol. 9, No. 1, 1971, pp. 91–100.

[8]Shakhore, E. M., "Rarefied Gas Flow Over a Plate Parallel to the Stream" *USSR Fluid Dynamics*, 1973, pp. 119–126.

[9]Beottcher, R. D., Koppenwallner, G., and Legge, H., "Flat Plate Skin Friction in the Range Between Hypersonic Continuum and Free Molecular Flow," *Proceedings of the 10th International Symposium on Rarefied Gas Dynamics*, Aspen, CO, Vol. 1, 1976, pp. 348–359.

[10]Hermina, W. L., "Monte Carlo Simulation of Rarefied Flow Along a Flat Plate," AIAA Paper 87-1547, June 1987.

[11]Allegre, J., and Bisch, C., "Angle of Attack and Leading Edge Effects on the Flow about a Flat Plate at Mach Number 18," *AIAA Journal*, Vol. 6, No. 5, 1968, pp. 848–852.

[12]Gai, S. L., "An Experimental Study of the Flow Past a Flat Plate at Incidence in Supersonic Low Density Stream," *Rarefied Gas Dynamics*, edited by H. Oguchi, Vol. 1, Univ. of Tokyo Press, Tokyo, 1984, pp. 257–264.

[13]Cheng, H. K., and Wong, E., "Fluid Dynamic Modeling and Numerical Simulation of Low-Density Hypersonic Flows," AIAA Paper 88-2731, June 1988.

[14]Bird, G. A., "Monte Carlo Simulation in an Engineering Context," *AIAA Progress in Astronautics and Aeronautics: Rarefied Gas Dynamics*, Vol. 74, P. 1, edited by Sam S. Fisher, 1981, pp. 235–239.

[15]Bird, G. A., *Molecular Gas Dynamics*, Clarendon Press, Oxford, 1976.

[16]Jacchia, L. C., "Thermospheric Temperature Density and Composition: New Models," *Research in Space Science*, SAO Special Rept. 375, March 1977.

[17]Moss, J. N., and Bird, G. A., "Direct Simulation of Transitional Flow for Hypersonic Reentry Conditions," *Thermal Design of Aeroassisted Orbital Transfer Vehicles*, edited by H. F. Nelson, Vol. 96, Progress in Astronautics and Aeronautics, AIAA, 1985, pp. 113–139.

[18]Dogra, V. K., Moss, J. N., and Simmonds, A. L., "Direct Simulation of Aerothermal Loads for an Aeroassist Flight Experiment Vehicle," AIAA Paper 87-1546, June 1987.

[19]Biolsi, L., Private communications, Department of Chemistry, Univ. of Missouri-Rolla, Rolla, MO.

[20]Blanchard, R. C., and Buck, G. M., "Rarefied-Flow Aerodynamics and Thermosphere Structure from Shuttle Flight Measurements," *Journal of Spacecraft and Rockets*, Vol. 23. No. 1, 1986.

[21]Bird, G. A., "Application of the Direct Simulation Monte Carlo Method to the Full Shuttle Geometry," AIAA Paper 90-1692, June 1990.